Nanochannel-Directed Growth of Multi-Segment Nanowire Heterojunctions of Metallic $Au_{1-x}Ge_x$ and Semiconducting Ge

Xiangdong Li,[†] Guowen Meng,[*,†] Shengyong Qin,[‡] Qiaoling Xu,[†] Zhaoqin Chu,[†] Xiaoguang Zhu,[†] Mingguang Kong,[†] and An-Ping Li[*,‡]

[†]Key Laboratory of Materials Physics and Anhui Key Laboratory of Nanomaterials and Nanostructures, Institute of Solid State Physics, Chinese Academy of Sciences, Hefei 230031, People's Republic of China, and [‡]Center for Nanophase Materials Sciences, Oak Ridge National Laboratory, Oak Ridge, Tennessee 37831, United States

ABSTRACT

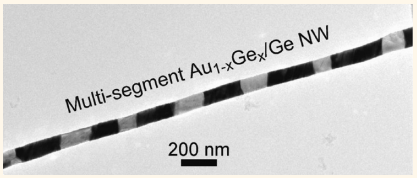

We report on the synthesis of multi-segment nanowire (NW) junctions of $Au_{1-x}Ge_x$ and Ge inside the nanochannels of porous anodic aluminum oxide template. The one-dimensional heterostructures are grown with a low-temperature chemical vapor deposition process, assisted by electrodeposited Au nanowires (AuNWs). The Au-catalyzed vapor–liquid–solid growth process occurs simultaneously in multiple locations along the nanochannel, which leads to multi-segment $Au_{1-x}Ge_x$/Ge heterojunctions. The structures of the as-grown hybrid NWs, analyzed by using transmission electron microscopy and energy-dispersive X-ray spectroscopy elemental mapping, show clear compositional modulation with variable modulation period and controllable junction numbers. Remarkably, both GeNW and $Au_{1-x}Ge_x$NW segments are single crystalline with abrupt interfaces and good crystallographic coherences. The electronic and transport properties of individual NW junctions are measured by using a multi-probe scanning tunneling microscope, which confirms the semiconducting nature of Ge segments and the metallic behavior of $Au_{1-x}Ge_x$ segments, respectively. The high yield of multiple segment NW junctions of a metal–semiconductor can facilitate the applications in nanoelectronics and optoelectronics that harness multiple functionalities of heterointerfaces.

KEYWORDS: germanium · gold · multiple segment hybrid nanowires · electrodeposition · chemical vapor deposition

One-dimensional (1D) multiple segment nanostructures that contain heterojunctions between various metals and semiconductors are of great interest due to their fascinating chemistry and size-, shape-, and material-dependent properties.[1−6] Multi-segment nanowire (NW) junctions of a ferromagnetic metal (*e.g.*, Fe or Co) alternated with a nonmagnetic metal are shown to exhibit giant magnetoresistance and proposed as nanosensors.[5,6] Semiconductor superlattice NWs are reported to display unique photonic and electronic properties and suggested as nanobarcodes and polarized nanoscale light-emitting diodes.[1] Metal/semiconductor multi-segment NWs are demonstrated to have unique electronic, optical, and magnetic properties and are recommended as nanoelectronics,[7] sensors,[8] and optics.[9]

To utilize these hybrid nanojunctions in device applications, good control to the interface sharpness and the crystalline quality of individual segments of different nanomaterials is required. In this regard, various bottom-up methods have been developed to build multi-segment hybrid NWs. For example, sequential electrochemical deposition was used to grow metal–metal microrods,[10] pulse electrodeposition was used to grow Ni/Pt and Au/Co multilayered NWs,[5,11] and a colloidal route was used to synthesize CdS–Ag_2S nanorod superlattices through partial cation exchange.[12] However, these methods usually produce polycrystalline products with less than ideal interfaces.[13] To improve the crystalline quality, metal-catalyzed vapor–liquid–solid (VLS) approach was used to grow semiconducting GaAs/GaP and Si/SiGe NW superlattices,[1,13] and combinatorial electrochemical deposition and subsequent chemical vapor deposition (CVD) was used to synthesize two-segment metal NW/Si NW heterostructures.[14] However, neither of them can be used to build multiple segment hybrid NWs of metal and semiconductor. In a pioneer work of synthesizing the multi-segment metal/semiconductor NWs, thermal diffusion of metals into SiNWs was used to form NiSi/Si NW superlattices.[7]

* Address correspondence to gwmeng@issp.ac.cn, apli@ornl.gov.

Received for review November 9, 2011 and accepted December 23, 2011.

Published online December 23, 2011
10.1021/nn2043466

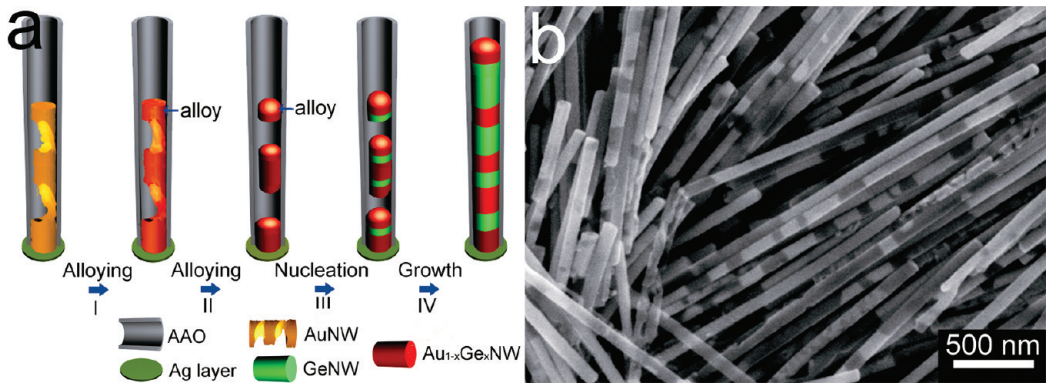

Figure 1. Multi-segment hybrid NWs of $Au_{1-x}Ge_x$ and Ge. (a) Schematic showing the formation of the multi-segment $Au_{1-x}Ge_x$/Ge NWs *via* a simultaneous multi-location Au-catalyzed VLS mechanism confined in one channel of the AAO template. (b) SEM image of multi-segment $Au_{1-x}Ge_x$/Ge NWs after the AAO template removal.

This fabrication process, however, suffers from its complexity, where CVD synthesized SiNWs have to be achieved first, and then SiNWs with the desired density are transferred onto a substrate, followed by selectively coating the SiNWs with Ni metal *via* photoresist and lithography, and last rapid thermal annealing in ambient N_2/H_2 to allow Ni thermal intrusion into the SiNWs to form NiSi/Si heterostructures.

Here we grow multi-segment hybrid NWs of $Au_{1-x}Ge_x$ and Ge inside the nanochannels of porous anodic aluminum oxide (AAO) template, with electrodeposited discontinuous AuNWs as catalyst. The GeNW segments are grown with CVD in a Au-catalyzed VLS process, and the $Au_{1-x}Ge_x$NW segments are formed simultaneously by *in situ* transforming the pure Au into $Au_{1-x}Ge_x$. The heterojunctions are shown to have good crystalline quality and sharp interfaces. This process thus provides a simple route toward the high-yield production of metal–semiconductor multi-segment NW heterojunctions.

RESULTS AND DISCUSSION

To explore the synthesis process of 1D metal–semiconductor heterojunctions, we choose the Au–Ge system (Figure S1, Supporting Information) with the following considerations: Au is proven to be a good catalyst for Ge growth,[15] and the eutectic Au–Ge alloys are metallic and can be used as interconnect/contact materials in Si-based semiconductor devices.[16] We grow the multi-segment hybrid NWs of eutectic alloy $Au_{1-x}Ge_x$ alternated with element Ge inside the nanochannels of the AAO template. The AAO template was fabricated by using an anodic anodization process.[17] After the fabrication of a free-standing AAO template, a silver film (~200 nm) was first sputtered onto one planar surface of the AAO template to serve as working electrode, and discontinuous AuNWs were then electrodeposited inside the nanochannels of the AAO by using a high electrical current density.[18] Note, it is usually hard to obtain multiple discontinuously sections of AuNWs inside the nanochannels in a conventional electrodeposition process. However, by using a much higher current density during the electrodeposition, we can modulate the diameters along the AuNW, namely, some sections having much smaller diameters than others, in the nanochannels of the AAO template. The detailed scanning electron microscopy observations on AuNWs grown at different current densities are shown in Figure S2a–c, Supporting Information. Furthermore, the AuNWs have a variable gap width between the AuNWs and the channel walls of the AAO template, small in the large-diameter sections and larger in the smaller-diameter sections. In the subsequent CVD growth process, the gaseous GeH_4 species can penetrate through these gaps and come into the smaller-diameter NW sections and grow the GeNWs. The AAO template embedded with the discontinuous AuNWs (Figure S2d, Supporting Information) was finally placed in an alumina tube furnace for CVD growth of element GeNWs and simultaneous *in situ* transformation of Au into eutectic alloy $Au_{1-x}Ge_x$.

The growth process of multi-segment NWs of $Au_{1-x}Ge_x$ and Ge inside a nanochannel of the AAO template is schematically shown in Figure 1a with four growth stages. (I) The pure metal AuNW is transformed into a non-uniform-diameter Au–Ge alloy NW due to the adsorption of GeH_4 species into the exposed surface of the AuNW.[19] (II) With the increase of Ge species adsorption, the NW is first liquefied completely in smaller-diameter sections, which breaks the NW into discontinuous sections due to a surface tension effect. (III) Continuous supply of Ge species results in the supersaturation of the surface liquid layers of the alloy NW, and the nucleation and growth of Ge nanocrystals occur in the empty sections driven by VLS growth mechanism. In the meantime, Ge species from the newly formed GeNWs can also diffuse into the solid AuNW segments during the whole growth process and gradually transform the solid Au into eutectic alloy $Au_{1-x}Ge_x$. (IV) Further growth of GeNWs joins the discontinuous sections together, followed by reconstruction

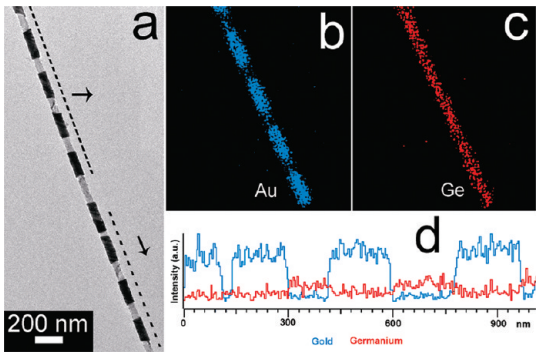

Figure 2. Multi-segment hybrid NWs of $Au_{1-x}Ge_x$ and Ge. (a) TEM image of a typical multi-segment $Au_{1-x}Ge_x$/Ge NW. (b,c) Elemental mapping showing the spatial distribution of Au (red) and Ge (green), respectively, in the hybrid NWs. (d) Line profiles of the composition through the portion of multi-segment $Au_{1-x}Ge_x$/Ge NW, showing the change in composition as a function of the distance. The weak periodic-like variation in the spatial distribution of Ge (c) and the low Ge signal (shown red) in the line profiles of GeNW segments (d) due to that the GeNW segments are partially etched during the removal of the AAO template in an aqueous NaOH solution.

to form a multi-segment $Au_{1-x}Ge_x$/Ge NW with flat interfaces.[20] After removing the AAO template in a NaOH aqueous solution, multi-segment hybrid NWs can be obtained, as shown in the SEM image of Figure 1b with alternating light and dark contrasts.

Morphological characteristics of the as-grown multi-segment hybrid NWs were first examined by using a transmission electron microscopy (TEM). Figure 2a is a TEM image of a single multi-segment hybrid NW, displaying a quasi-periodic variation in contrasts, as well as abrupt interfaces and good continuity between adjacent segments. The corresponding energy-dispersive X-ray spectroscopy (EDS) elemental mapping (Figure 2b,c) reveals that the dark contrast segment is composed of a Au-rich Au−Ge alloy, while the light contrast segment is mainly composed of Ge (red in color) with a very little amount of Au (blue in color) homogeneously distributed. Due to the negligible solid solubility of Au in Ge at low growth temperatures,[21] the doping level of Ge in the AuNW segment (dark contrast) is much higher than that of Au in the GeNW segment (light contrast). As indicated in the line profile analysis shown in Figure 2d, these hybrid NWs are compositionally modulated with a remarkable modulation period.

The interfacial microstructures were investigated on a representative multi-segment $Au_{1-x}Ge_x$/Ge NW. Figure 3a shows that the NW has uniform diameter with an abrupt interface between the adjacent two segments. Lattice-resolved image taken on a junction region (Figure 3b) indicates that both adjacent segments are single crystalline and the abrupt interface shows good adherence, which can be ascribed to the interdiffusion of atomic Ge and Au.[1,22] The corresponding selected area electron diffraction (SAED) pattern

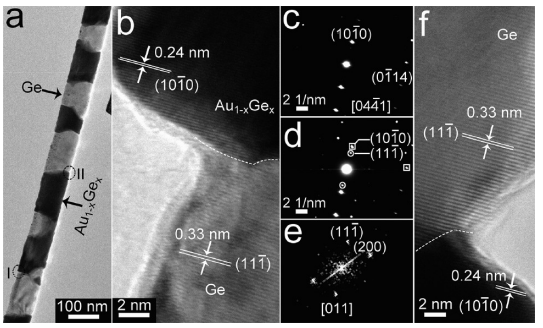

Figure 3. Microstructures of the multi-segment $Au_{1-x}Ge_x$/Ge NW. (a) TEM image of a typical multi-segment $Au_{1-x}Ge_x$/Ge NW. (b) HRTEM image taken from the junction region (marked region I in (a)). (c) SAED pattern taken from the $Au_{1-x}Ge_x$NW segment. (d) SAED pattern including both GeNW and $Au_{1-x}Ge_x$NW segments (the spots of Ge are marked by circles; the spots of $Au_{1-x}Ge_x$ are marked by rectangles). (e) Reciprocal lattices determined from two-dimensional Fourier transform of the lattice-resolved image of the GeNW segment. (f) HRTEM image taken from another junction region (marked region II in (a)).

taken from the $Au_{1-x}Ge_x$NW segment (Figure 3c) can be indexed to the $[04\bar{4}1]$ zone axis of the hexagonal crystal $Au_{0.72}Ge_{0.28}$ (JCPDS 07-1022) (Figure S3, Supporting Information), confirming that the $Au_{1-x}Ge_x$NW segment grows perpendicularly to the $(10\bar{1}0)$ plane. The chemical composition of $Au_{1-x}Ge_x$ is $x \sim 0.28$, according to the Au−Ge phase diagram (Figure S1, Supporting Information). The reciprocal lattice peaks determined from two-dimensional Fourier transform of the lattice-resolved image of the GeNW segment (Figure 3e) can be indexed to the [011] zone axis of face-centered cubic (fcc) Ge (JCPDS 04-0545) (Figure S3, Supporting Information), and the $[11\bar{1}]$ direction is aligned with the axis, demonstrating the $[11\bar{1}]$ growth direction. The SAED pattern (Figure 3d) including both GeNW and $Au_{1-x}Ge_x$NW segments show that the $(10\bar{1}0)$ plane of $Au_{1-x}Ge_x$ (marked by rectangle) is nearly parallel to the $(11\bar{1})$ plane of Ge (marked by circle), being consistent with the corresponding lattice-resolved image (Figure 3b). Similar results have been obtained in another junction between the $Au_{1-x}Ge_x$NW and GeNW segments, as clearly shown in Figure 3f, where the corresponding lattice-resolved image taken from the junction region shows that the $Au_{1-x}Ge_x$NW and GeNW segments are longitudinally connected with abrupt interface and good adherence, and the $(10\bar{1}0)$ plane of $Au_{1-x}Ge_x$ is nearly parallel to the $(11\bar{1})$ plane of Ge. The fixed crystalline registration is presumably corresponding to a minimized interface lattice mismatch, which is formed in the cooling stage when the $Au_{1-x}Ge_x$ changed from the liquid to solid state.[23]

To further study the crystalline orientations of multi-segment $Au_{1-x}Ge_x$/Ge NWs, we examined another two $Au_{1-x}Ge_x$NW segments in an $Au_{1-x}Ge_x$/Ge NW (Figure S4a, Supporting Information). As shown in Figure S4b,c Supporting Information, respectively, one $Au_{1-x}Ge_x$NW

segment grows along the [$\bar{1}10\bar{2}$], while another grows along the [$21\bar{3}\bar{3}$]; namely, the two $Au_{1-x}Ge_x$NW segments in the same multi-segment $Au_{1-x}Ge_x$/Ge NW have different growth directions. It appears that these two GeNW segments are catalyzed by two different catalysts that have different crystalline orientations. However, as the orientation of the $Au_{1-x}Ge_x$NW is primarily determined by the initial growth process of non-uniform AuNWs, there is still a good chance that all interfaces have the same crystalline registration relationship along the same multi-segment NW.

A control experiment was performed to examine whether the formation of multi-segment NWs of $Au_{1-x}Ge_x$ and Ge is due to the discontinuous Au catalysts or merely an effect of phase segregation.[24] Under the same CVD conditions as the multi-segment NWs, we grew several hybrid NWs by using the electrodeposited highly dense AuNWs (Figure S5, Supporting Information) as catalyst. Without diameter modulations along the AuNW, most of the as-grown NWs only have two segments, $Au_{1-x}Ge_x$ and Ge. SEM observation (Figure 4a) on the cross section of a piece of AAO template after the CVD process shows two-segment NWs with clear contrasts inside the porous AAO template. TEM images of typical two-segment NWs (Figure 4b,c) after template removal display an abrupt interface and good adherence between the two segments. The corresponding EDS elemental mapping (Figure 4d,e) confirms that the light contrast segment is mainly composed of Ge (red in color), while the dark contrast segment is composed of the Au-rich Au−Ge alloy. The Ge segment is shown to be single crystalline with [200] growth direction, and the $Au_{1-x}Ge_x$ segment is single crystalline too with a hexagonal crystal $Au_{0.72}Ge_{0.28}$ and [$01\bar{1}2$] growth direction (Figure S6, Supporting Information). So, highly dense AuNWs lead to two-segment $Au_{1-x}Ge_x$/Ge hybrid NWs, where the GeNW is inclined to nucleate on the top of dense AuNW (detailed growth process of two-segment $Au_{1-x}Ge_x$/Ge NW heterostructures can be found in Figure S7), while discontinuous or dotted-line-like AuNWs lead to multi-segment hybrid NWs of $Au_{1-x}Ge_x$ alternated with Ge. Therefore, the more discontinuous sections the electrodeposited AuNWs have, the more segments the resultant multi-segment hybrid NWs will be composed of.

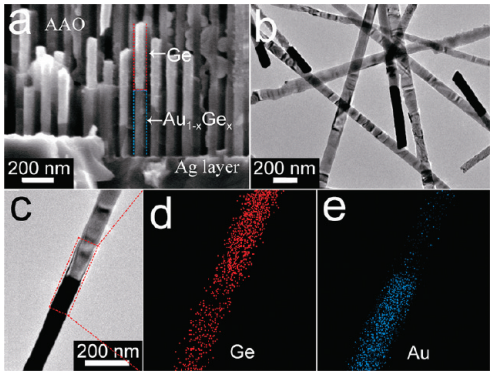

Figure 4. Two-segment $Au_{1-x}Ge_x$/Ge NWs. (a) SEM image of the two-segment $Au_{1-x}Ge_x$/Ge NWs embedded in the nanochannels of the AAO template. (b) TEM image of several two-segment $Au_{1-x}Ge_x$/Ge NWs. (c) Enlarged TEM image of a single two-segment $Au_{1-x}Ge_x$/Ge NW. (d, e) Elemental mapping taken from part of the NW including the interface of the two segments.

The electronic properties of the segmented NWs are examined by using a four-probe scanning tunneling microscope (STM),[25] after dispersing the NWs onto a SiO_2/Si substrate. Under the guidance of an *in situ* scanning electron microscope (SEM), the STM tip is located precisely on $Au_{1-x}Ge_x$ and Ge segments to measure the scanning tunneling spectroscopy (STS) at different locations (Figure 5a). As shown in Figure 5b,c, the tunneling *I*(*V*) and d*I*/d*V* curves measured on the $Au_{1-x}Ge_x$ segment show finite conductance near 0 V, which indicates that the electronic density of state is

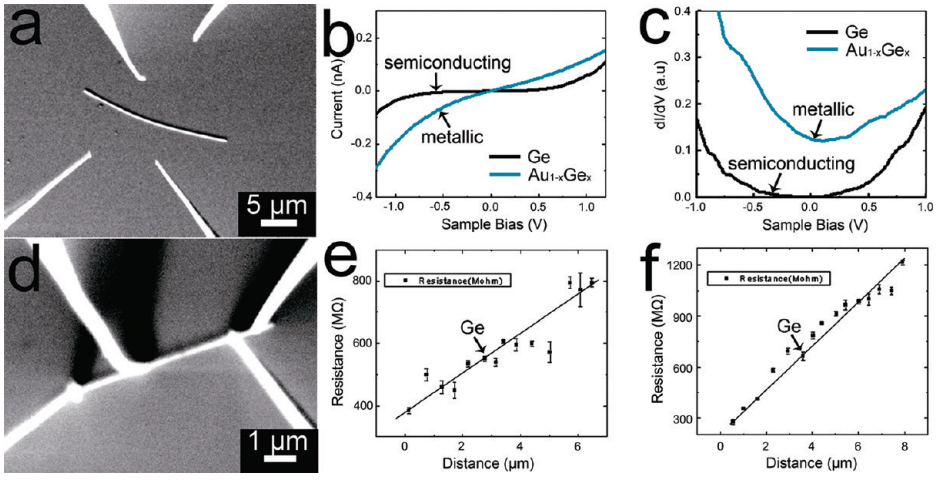

Figure 5. Transport properties of Ge and $Au_{1-x}Ge_x$ segments. (a) SEM image of a single NW. (b, c) Averaged tunneling *I*(*V*) curves and derivative conductance (d*I*/d*V*) curves measured on a single Ge and $Au_{1-x}Ge_x$ segments, respectively. (d) SEM image of a NW being contacted with four tips. (e, f) Resistance dependence on the probe spacing.

finite near the Fermi level; namely, the segment has a metallic conductance nature. In contrast, the STS data taken on the Ge segment display an energy gap near the Fermi level. The band gap width is found to change between 0.2 and 0.5 eV from location to location, with the Fermi level located near the middle of the band gap. Furthermore, the resistance of the semiconducting segment is measured by locating multiple STM tips on the same NWs with variable probe spacing (Figure 5d). As shown in Figure 5e,f, the resistance (R) scales almost linearly with the probe spacing (L) at room temperature, indicating a diffusive type of conductance behavior. The resistivity of the NW can be extrapolated from the slope of the $R(L)$ scaling. The obtained resistivity varies from sample to sample in the range of 30−67 Ωcm. It is noted that the Ge surface is covered with a thin layer (<1 nm) of residue oxide, as shown in Figure 3b. A band gap measured on the Ge part of wire may consist of contributions from both Ge and surface oxide. However, the measured band gap (0.2−0.5 eV) is much smaller than that of GeO_x (4−6 eV),[26] thus this band gap should mainly reflect the contribution from Ge itself. The location of the Fermi level near the middle of band gap suggests that Ge is nearly pure or high compensated, consistent with the report in ref 24 and the high resistivity results in Figure 5e,f.

CONCLUSIONS

In conclusion, multi-segment hybrid NWs of $Au_{1-x}Ge_x$ and Ge with abrupt interfaces and good adherences have been fabricated by using a CVD process catalyzed by the electrodeposited discontinuous AuNWs inside partial nanochannels of the AAO template. The Ge segments are formed *via* the Au-catalyzed VLS growth process, and the $Au_{1-x}Ge_x$ segments are achieved simultaneously *via* diffusion-driven *in situ* transformation of the pure Au into $Au_{1-x}Ge_x$. Both Ge and $Au_{1-x}Ge_x$ segments are single crystalline, but the lattice registration between the two varies from NW to NW. Transport properties are examined by using a four-probe STM which confirms the hybrid semiconductor and metal nature of the NWs. The numbers of semiconductor/metal junctions can be tuned by controlling the density of discontinuous electrodeposited AuNWs. The approaches to multi-segment hybrid NWs of metallic $Au_{1-x}Ge_x$ and semiconducting Ge by controlling the morphology of electrodeposited AuNWs rather than periodically changing the precursors might be applicable to other multi-segment hybrid NWs of eutectic alloy and semiconductor and have potentials for the future nanoelectronics, nanodevices, and nanosystems.

METHODS

Preparation of the AAO Template. The AAO templates were synthesized *via* a two-step anodization of high-purity aluminum foils at 50 V.[27]

Electrodeposition of AuNWs. Prior to electrodeposition of Au, a silver film (~200 nm) was sputtered onto one planar surface side of the AAO template to serve as working electrode. Then the electrodeposition of non-uniform-diameter AuNWs was performed under a cathode current density of 30 μA/cm^2 for 6 h in an aqueous solution containing 12 g/L $HAuCl_4$, 160 g/L Na_2SO_3, 5 g/L EDTA, and 30 g/L K_2HPO_4,[28] while electrodeposition of highly dense AuNWs was performed under a low cathode current density of 6 μA/cm^2 for 3 h.

CVD of Multi-Segment Hybrid NWs. Ge nanoarchitectures were fabricated using a low-temperature atmospheric pressure CVD process. First, the AAO template with electrodeposited Au in the nanochannels was loaded with a ceramic boat into the center zone of a horizontal quartz tube furnace. The quartz tube was first pumped using a mechanical pump and purged by high-purity Ar for two cycles. Then the furnace was heated to growth temperature under a 60 sccm flow of Ar at a heating rate of 10 °C/min. For the two- and multi-segment hybrid NWs of $Au_{1-x}Ge_x$ and Ge, the growth was performed under a 60 sccm flow of Ar in tandem with an 8 sccm flow of GeH_4 (5% GeH_4 in H_2) at 340 °C for 4 h.

Characterization. The as-prepared samples were released by dissolving the AAO templates in a 1 M NaOH aqueous solution for 8 h at room temperature and then washed repeatedly with deionized water. The morphologies and structures of the as-prepared samples were characterized by using X-ray diffraction (XRD, Philips, X'Pert Pro MPD, with Cu Kα irradiation), scanning electron microscopy (SEM, Sirion 200, FEI, at 5 kV) with energy-dispersive X-ray spectroscopy (EDS OXFORD), transmission electron microscopy (TEM), and high-resolution TEM (HRTEM, JEOL2010 at 200 kV).

Acknowledgment. A portion of this research was conducted at the Center for Nanophase Materials Sciences, which is sponsored at Oak Ridge National Laboratory by the Office of Basic Energy Sciences, U.S. Department of Energy. The work was financially supported by the National Natural Science Foundation of China (Grant Nos. 50525207 and 50972145), National Basic Research Program of China (Grant No. 2007CB936601), and China Postdoctoral Science Foundation funded project (No. 2011M501069).

Supporting Information Available: Additional microstructural characterizations of the resultant nanoarchitectures. This material is available free of charge *via* the Internet at http://pubs.acs.org.

REFERENCES AND NOTES

1. Gudiksen, M. S.; Lauhon, L. J.; Wang, J. F.; Smith, D. C.; Lieber, C. M. Growth of Nanowire Superlattice Structures for Nanoscale Photonics and Electronics. *Nature* **2002**, *415*, 617–620.
2. Mieszawska, A. J.; Jalilian, R.; Sumanasekera, G. U.; Zamborini, F. P. The Synthesis and Fabrication of One-Dimensional Nanoscale Heterojunctions. *Small* **2007**, *3*, 722–756.
3. Hu, J. Q.; Bando, Y.; Zhan, J. H.; Golberg, D. Fabrication of Silica-Shielded Ga−ZnS Metal Semiconductor Nanowire Heterojunctions. *Adv. Mater.* **2005**, *17*, 1964–1969.
4. Zhan, J. H.; Bando, Y.; Hu, J. Q.; Liu, Z. W.; Yin, L. W.; Golberg, D. Fabrication of Metal−Semiconductor Nanowire Heterojunctions. *Angew. Chem., Int. Ed.* **2005**, *44*, 2140–2144.
5. Valizadeh, S.; Hultman, L.; George, J. M.; Leisner, P. Template Synthesis of Au/Co Multilayered Nanowires by Electrochemical Deposition. *Adv. Funct. Mater.* **2002**, *12*, 766–772.
6. Anguelouch, A.; Reich, D. H.; Chien, C. L.; Tondra, M. Detection of Ferromagnetic Nanowires Using GMR Sensors. *IEEE Trans. Magn.* **2004**, *40*, 2997–2999.

7. Wu, Y.; Xiang, J.; Yang, C.; Lu, W.; Lieber, C. M. Single-Crystal Metallic Nanowires and Metal/Semiconductor Nanowire Heterostructures. *Nature* **2004**, *430*, 61–65.
8. Wang, X.; Ozkan, C. S. Multisegment Nanowire Sensors qfor the Detection of DNA Molecules. *Nano Lett.* **2008**, *8*, 398–404.
9. Pena, D. J.; Mbindyo, J. K. N.; Carado, A. J.; Mallouk, T. E.; Keating, C. D.; Razavi, B.; Mayer, T. S. Template Growth of Metal−CdSe−Metal Nanowires. *J. Phys. Chem. B* **2002**, *106*, 7458–7462.
10. Nicewarner-Pena, S. R.; Freeman, R. G.; Reiss, B, D.; He, L.; Pena, D. J.; Walton, I. D.; Cromer, R.; Keating, C. D.; Natan, M. J. Submicrometer Metallic Barcodes. *Science* **2001**, *294*, 137–141.
11. Liang, H. P.; Guo, Y. G.; Hu, J. S.; Zhu, C. F.; Wan, L. J.; Bai, C. L. Ni−Pt Multilayered Nanowire Arrays with Enhanced Coercivity and High Remanence Ratio. *Inorg. Chem.* **2005**, *44*, 3013–3015.
12. Robinson, R. D.; Sadtler, B.; Demchenko, D. O.; Erdonmez, C. K.; Wang, L. W.; Alivisatos, A. P. Spontaneous Superlattice Formation in Nanorods through Partial Cation Exchange. *Science* **2007**, *317*, 355–358.
13. Wu, Y. Y.; Fan, R.; Yang, P. D. Block-by-Block Growth of Single-Crystalline Si/SiGe Superlattice Nanowires. *Nano Lett.* **2002**, *2*, 83–86.
14. Luo, J.; Zhu, J. Arrays of One-Dimensional Metal/Silicon and Metal/Carbon Nanotube Heterojunctions. *Nanotechnology* **2006**, *17*, S262–S270.
15. Li, X. D.; Meng, G. W.; Xu, Q. L.; Kong, M. G.; Zhu, X. G.; Chu, Z. Q.; Li, A. P. Controlled Synthesis of Germanium Nanowires and Nanotubes with Variable Morphologies and Sizes. *Nano Lett.* **2011**, *11*, 1704–1709.
16. Soma, T.; Ayyub, P.; Kabiraj, D.; Kulkarni, N.; Kulkarni, V. N.; Avasthi, D. K. Formation of $Au_{0.6}Ge_{0.4}$ Alloy Induced by Au-Ion Irradiation of Au/Ge Bilayer. *J. Appl. Phys.* **2003**, *93*, 903–906.
17. Li, A.-P.; Muller, F.; Birner, A.; Nielsch, K.; Gosele, U. Hexagonal Pore Arrays with a 50−420 nm Interpore Distance Formed by Self-Organization in Anodic Alumina. *J. Appl. Phys.* **1998**, *84*, 6023–6026.
18. Meng, G. W.; Han, F. M.; Zhao, X. L.; Chen, B. S.; Yang, D. H.; Liu, J. X.; Xu, Q. L.; Kong, M. G.; Zhu, X. G.; Jung, Y. J.; *et al.* A General Synthetic Approach to Interconnected Nanowire/Nanotube and Nanotube/Nanowire/Nanotube Heterojunctions with Branched Topology. *Angew. Chem., Int. Ed.* **2009**, *48*, 7166–7170.
19. Wu, Y. Y.; Yang, P. D. Direct Observation of Vapor−Liquid−Solid Nanowire Growth. *J. Am. Chem. Soc.* **2001**, *123*, 3165–3166.
20. Wang, W.; Lu, X. L.; Zhang, T.; Zhang, G. Q.; Jiang, W. J.; Li, X. G. Bi_2Te_3/Te Multiple Heterostructure Nanowire Arrays Formed by Confined Precipitation. *J. Am. Chem. Soc.* **2007**, *129*, 6702–6703.
21. Holmberg, V. C.; Panthani, M. G.; Korgel, B. A. Phase Transitions, Melting Dynamics, and Solid-State Diffusion in a Nano Test Tube. *Science* **2009**, *326*, 405–407.
22. Lu, K. C.; Wu, W. W.; Wu, H. W.; Tanner, C. M.; Chang, J. P.; Chen, L. J.; Tu, K. N. *In Situ* Control of Atomic-Scale Si Layer with Huge Strain in the Nanoheterostructure NiSi/Si/NiSi through Point Contact Reaction. *Nano Lett.* **2007**, *7*, 2389–2394.
23. Ding, Y.; Wang, Z. L. Structure Analysis of Nanowires and Nanobelts by Transmission Electron Microscopy. *J. Phys. Chem. B* **2004**, *108*, 12280–12291.
24. Chueh, Y. L.; Boswell, C. N.; Yuan, C. W.; Shin, S. J.; Takei, K.; Ho, J. C.; Ko, H.; Fan, Z. Y.; Haller, E. E.; Chrzan, D. C.; *et al.* Nanoscale Structural Engineering *via* Phase Segregation: Au−Ge System. *Nano Lett.* **2010**, *10*, 393–397.
25. Kim, T. H.; Wang, Z. H.; Wendelken, J. F.; Weitering, H. H.; Li, W. Z.; Li, A. P. A Cryogenic Quadraprobe Scanning Tunneling Microscope System with Fabrication Capability for Nanotransport Research. *Rev. Sci. Instrum.* **2007**, *78*, 123701.
26. Lin, L.; Xiong, K.; Robertson, J. Atomic Structure, Electronic Structure, and Band Offsets at Ge:GeO:GeO_2 Interfaces. *Appl. Phys. Lett.* **2010**, *97*, 242902.
27. Masuda, H.; Fukuda, K. Ordered Metal Nanohole Arrays Made by a Two-Step Replication of Honeycomb Structures of Anodic Alumina. *Science* **1995**, *268*, 1466–1468.
28. Zhang, X. Y.; Zhang, L. D.; Lei, Y.; Zhao, L. X.; Mao, Y. Q. Fabrication and Characterization of Highly Ordered Au Nanowire Arrays. *J. Mater. Chem.* **2001**, *11*, 1732–1734.